Estimating the capture and loss of cold plasma from ionospheric outflow

S. Haaland,[1,2] A. Eriksson,[3] E. Engwall,[3] B. Lybekk,[4] H. Nilsson,[5] A. Pedersen,[4] K. Svenes,[6] M. André,[3] M. Förster,[7] K. Li,[1,8] C. Johnsen,[2] and N. Østgaard[2]

Received 1 March 2012; revised 3 May 2012; accepted 30 May 2012; published 18 July 2012.

[1] An important source of magnetospheric plasma is cold plasma from the terrestrial ionosphere. Low energy ions travel along the magnetic field lines and enter the magnetospheric lobes where they are convected toward the tail plasma sheet. Recent observations indicate that the field aligned ion outflow velocity is sometimes much higher than the convection toward the central plasma sheet. A substantial amount of plasma therefore escapes downtail without ever reaching the central plasma sheet. In this work, we use Cluster measurements of cold plasma outflow and lobe convection velocities combined with models of the magnetic field in an attempt to determine the fate of the outflowing ions and to quantify the amount of plasma lost downtail. The results show that both the circulation of plasma and the direct tailward escape of ions varies significantly with magnetospheric conditions. For strong solar wind driving with a southward interplanetary magnetic field, also typically associated with high geomagnetic activity, most of the outflowing plasma is convected to the plasma sheet and recirculated. For periods with northward interplanetary magnetic field, the convection is nearly stagnant, whereas the outflow, although limited, still persists. The dominant part of the outflowing ions escape downtail and are directly lost into the solar wind under such conditions.

Citation: Haaland, S., et al. (2012), Estimating the capture and loss of cold plasma from ionospheric outflow, *J. Geophys. Res.*, *117*, A07311, doi:10.1029/2012JA017679.

1. Introduction

[2] An important (and sometimes probably dominant) source of plasma supply to the terrestrial magnetosphere is outflow from the polar ionosphere (see reviews by, e.g., *Chappell et al.* [1987, 2000], *Yau and Andre* [1997], and *Moore and Horwitz* [2007]. Several important outflow source regions exist in the ionosphere; the polar wind, the ion cleft and the auroral region.

[3] *Axford* [1968] studied theoretical aspects of outflow of light ions (they mainly focused on escape of He^3 and He^4) from the polar cap regions (≥75° magnetic latitude), and suggested the term 'polar wind' to describe the outflow. In this region, ions are primarily accelerated upward by the electric field arising from charge separation set up by escaping photoelectrons or due to an ambipolar electric field caused by a pressure gradient of thermal electrons. Ionospheric outflow, in particular from the former process, is thus modulated by solar irradiance [*Laakso et al.*, 2002; *Kitamura et al.*, 2011]. Later, *Lockwood et al.* [1985b] presented a statistical study of O^+ outflow from the dayside ionosphere near the polar cap boundary. This outflow, often associated with outflow of lighter ions, was found to be dependent on both season and geomagnetic disturbance level. Still, this source, sometimes known as the cleft ion fountain [*Lockwood et al.*, 1985a], is probably the most dominating source of ion outflow from the polar cap. Even higher rates of ionospheric outflow have been observed in the nightside auroral region [e.g., *Yau et al.*, 1985].

[4] Several aspects of ion outflow, such as origin, composition, heating, mixing with plasma of solar origin as well as solar illumination control of the outflow rate has been also discussed more recently by, e.g., *Moore et al.* [1999].

[5] The low plasma density above the polar cap regions makes direct measurements with plasma instruments difficult. In addition to the low count rates, measurements are often severely affected by spacecraft charging. A spacecraft immersed in a thin plasma emits photoelectrons and will eventually be charged to large positive potentials. A

[1]Max-Planck Institute for Solar Systems Research, Katlenburg-Lindau, Germany.
[2]Department of Physics and Technology, University of Bergen, Bergen, Norway.
[3]Swedish Institute of Space Physics, Uppsala, Sweden.
[4]Department of Physics, University of Oslo, Oslo, Norway.
[5]Swedish Institute of Space Physics, Kiruna, Sweden.
[6]Norwegian Defence Research Establishment, Kjeller, Norway.
[7]Helmholtz Centre Potsdam, German Research Centre for Geosciences, Potsdam, Germany.
[8]Center for Space Science and Applied Research, Chinese Academy of Sciences, Beijing, China.

Corresponding author: S. Haaland, Department of Physics and Technology, University of Bergen, Allégaten 55, N-5007 Bergen, Norway. (stein.haaland@issi.unibe.ch)

0148-0227/12/2012JA017679

significant part of the low energy ion population will therefore be shielded from the detectors, and e.g., plasma moments will not be reliable. Studies of cold ion outflow at high altitudes are therefore rare. A notable exception is the study by *Su et al.* [1998]. They used ion moments from the Thermal Ion Dynamics Experiment (TIDE) onboard the POLAR spacecraft during a limited time period when the on board Plasma Source Instrument (PSI) [see *Moore et al.*, 1995, 1997] was operating and the spacecraft potential could be stabilized to a potential around 2V.

[6] Most of our recent knowledge about cold plasma in the high altitude polar cap and lobe region is therefore based on measurements from double probe instruments [see, e.g., *Escoubet et al.*, 1997a; *Pedersen et al.*, 1998, 2001; *Laakso et al.*, 2002; *Engwall et al.*, 2009a; *Haaland et al.*, 2012; *André and Cully*, 2012, and references therein].

[7] The Cluster spacecraft quartet, with its comprehensive set of instruments combined with novel techniques have provided new opportunities to obtain more accurate measurements of density [*Pedersen et al.*, 2001, 2008; *Lybekk et al.*, 2012] and flux of cold outflowing ions [*Engwall et al.*, 2006, 2009b, 2009a], in the high altitude polar cap and lobe regions of the Earth's magnetosphere. Cluster also provides a better coverage and more precise measurements of plasma convection in the magnetosphere [*Haaland et al.*, 2008, 2009] than earlier missions.

[8] Whereas the mechanisms, source regions and composition of ion outflow have been addressed in a number of studies, there is less quantitative information about the final fate of the outflowing cold ions. In this paper, we use a combination of spacecraft potential, wake electric field and convection measurements to assess the fate of outflowing cold ions from the polar cap region. Our results are based on convection velocity measurements from the Electron Drift Instrument (EDI) [see *Paschmann et al.*, 2001], combined with electron density measurements and outflow velocity measurements obtained from the Electric Field and Wave Experiment (EFW) [see *Gustafsson et al.*, 2001].

[9] This paper is organized as follows: Section 2 describes the method used to determine whether the outflowing ions escape downtail into the solar wind or end up in the plasma sheet. In section 3, we give a brief description of the EDI and EFW instruments and their data products, as well as an overview of auxiliary data used to establish solar wind conditions and the geomagnetic activity level. We also provide characteristics of the two main data sources for this study - the *Engwall et al.* [2009b] data set with ion outflow velocities and densities, and the *Haaland et al.* [2008] data set with lobe convection results. Thereafter, in section 4 we present the loss versus circulation ratio for various geomagnetic activity levels and solar wind conditions. Section 5 provides a further discussion some of the assumptions and implications of the results. Finally, section 6 summarizes the paper.

2. Methodology

[10] In addition to the gyration, an ion escaping the ionosphere is mainly governed by two forces in the Earth's magnetosphere; First there is the motion (and any acceleration) along the magnetic field. Secondly, the magnetic flux tubes themselves are convected as a result of the interaction between the solar wind and dayside magnetopause.

[11] Whether an ion escaping the polar cap ionosphere at a certain latitude is directly lost downtail into the solar wind or fed to the plasma sheet (recirculated) is thus a competition between the parallel outflow velocity and the field line convection speed. Ions escaping at lower latitudes, e.g., the auroral zone are less relevant in this balance, since they are on field lines already threading the plasma sheet.

[12] Consider an ion escaping the ionosphere along a field line which is open at time t_1 as illustrated in Figure 1a. The ion has a field aligned velocity $V_{\parallel}$ (and possibly an acceleration along the field line). This field line will convect toward the central plasma sheet and eventually reconnect at the distant neutral line after some time, t_3. The effective path of this particular ion will therefore be the trajectory marked as a dashed line in the figure. If the ion is still earthward of the distant neutral line at time t_3, it will be fed to the plasma sheet (where it may eventually be lost by some other process). Other ions starting simultaneously, but at higher latitudes or ions having larger parallel velocities and/or acceleration will be able to escape the magnetosphere directly into the solar wind, however.

[13] For a given outflow velocity, $V_{\parallel}$ and convection velocity $V_{\perp}$, we can then define a set of regions in the magnetosphere which will determine the fate of these ions. This is illustrated in Figures 1a and 1b. We can also map this area to the polar cap ionosphere and get an idea about the source areas of these regions, as illustrated in Figure 1c. Note that this figure is just a sketch to illustrate our model - the actual sizes and shapes of these regions depend on a number of factors, such as magnetospheric configuration, disturbance level, initial parallel velocities and the field aligned acceleration of the outflowing ions, as well as the convection velocity in the magnetosphere. The model also neglects the intermittency of magnetospheric dynamics, most notable during southward IMF, where substorms initiated inside $X = -100$ R_E may release plasma in the form of a plasmoid (see further discussion in section 5.2). The model should thus be regarded as providing a lower limit to the *direct* tailward escape of ionospheric ions, and not an actual estimate where all loss processes are incorporated.

[14] In the following, we will use a large data set with measurements of parallel velocities and a corresponding data set with convection measurements. In our model, the distant neutral line is located at $X = -100$ R_E, and we use the T01 magnetospheric field model [*Tsyganenko*, 2002a, 2002b] to find the foot point of the ions observed. A discussion about the motivation and validity of these assumptions is given in section 5.1. From the data, we will calculate average outflow and convection measurements, and use the above method to determine the fate of the outflowing ions as a function of geomagnetic conditions and solar wind conditions.

[15] Ion outflow and convection are rather slow processes - typical transport times from the ionosphere to the nightside magnetosphere can be several hours. In our model, we assume stationarity, but in reality, both convection velocity and the magnetic field configuration fluctuate on such timescales.

3. Data and Instrumentation

[16] The results presented here are primarily based on in-situ measurements from the Cluster quartet of spacecraft. Cluster is a four-spacecraft mission flying in a nearly 90° inclination elliptical polar orbit, with perigee at around 4 R_E

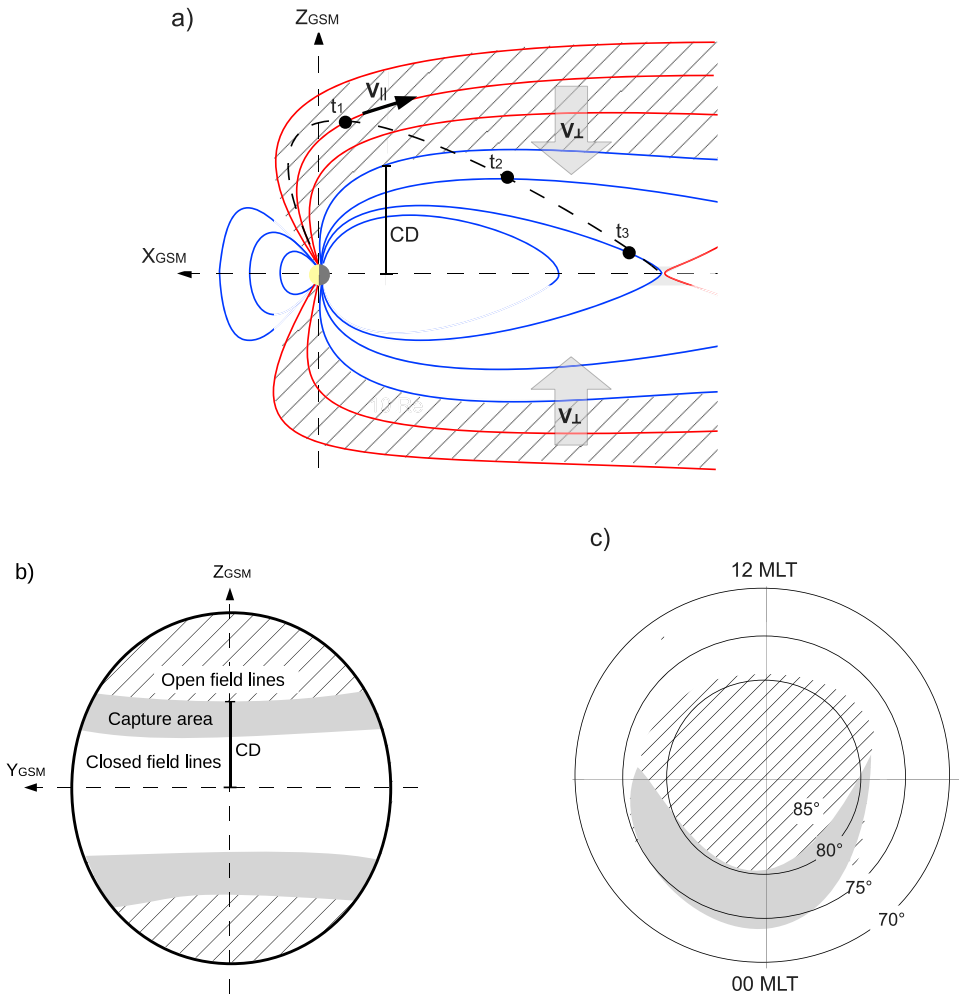

Figure 1. Definitions of open area (hatched), capture area (gray), trapped area (white) and convection distance (marked CD) in our model. (a) XZ view of the magnetosphere. An ion escaping the Earth's ionosphere at time t_1 will travel within a flux tube which is initially open (red lines). As time goes, this flux tube will convect through the lobes (t_2) toward the plasma sheet. During this time, the ion will also continue to travel and be accelerated tailward along the magnetic field. Eventually, at t_3, the field line will reconnect in the distant neutral line in the tail, and the ion will be on a closed field line and thus trapped (at least temporarily) in the magnetosphere. The effective gyro center trajectory of the ion will thus follow the dashed black line. Red lines on hatched background are open all the time it takes an ion to travel beyond the X-line. Ions within flux tubes threading this area are thus lost downtail. Blue lines are initially open, but during the time it takes for an ion to travel to the X-line, the field line will convect a distance CD toward the plasma sheet and the ions will eventually be captured in the plasma sheet. We refer to this area as the capture area. Ions flowing out at lower latitudes are on already closed field lines and will always recirculated in this model. (b) YZ cut through the tail at X = −10 R_E showing the three defined areas. (c) Foot points of the loss area and capture area in the polar cap.

and apogee around 20 R_E geocentric distance. The orbital period is approximately 57 hours - the spacecraft thus spend a significant time above the polar caps where the ion outflow can be detected, and in the magnetotail lobes where the convection can be measured.

[17] The instrumentation is identical on all four spacecraft, but not all instruments work on all spacecraft. In the science community, the four spacecraft are referred to as SC1, SC2, SC3 and SC4, and we use this notation to distinguish between the different spacecraft here. The two most relevant instruments for this paper are the electric field and wave instrument (EFW) [see *Gustafsson et al.*, 2001; *Pedersen et al.*, 2001]), and the electron drift instrument (EDI) [see *Quinn et al.*, 2001; *Paschmann et al.*, 2001]. EFW is operating on all four spacecraft (though we do not utilize data from all spacecraft - see section 3.1), and EDI is operating on SC1, SC2 (until April 2004) and SC3. More details about the Cluster mission and its comprehensive instrumentation can be found in *Escoubet et al.* [1997b].

[18] In addition to the in-situ observations from Cluster, we use measurements of the solar wind, interplanetary magnetic field (IMF) and solar irradiation as well as geomagnetic

indices to check correlations and dependencies. Some of these auxiliary data are also used for parametrization of the T01 magnetic field model.

[19] Below, we give a brief description of the data sets and their characteristics.

3.1. Cold Plasma Outflow Velocity and Density

[20] In order to estimate the average field aligned outflow velocity and corresponding flux, we have used the data set from *Engwall et al.* [2009a]. This data set consists of more than 1 million time tagged records of electron density and 3D plasma drift velocity, as well auxiliary parameters such as spacecraft position, solar wind and IMF information and geomagnetic disturbance indices.

[21] The technique of using the probe potential to obtain electron density is limited to cold plasma (energies up to approximately 100 eV) and does not allow for distinction between different ion species [*Pedersen et al.*, 2001, 2008]. A number of papers [see, e.g., *Moore and Horwitz*, 2007, and references therein] have pointed out that the cold outflow can have a large oxygen component, though.

[22] The outflow velocity and direction is calculated from measurements of the convection electric field and the observed spacecraft wake; In the cold tenuous plasma of the polar cap and lobe regions, the spacecraft potential energy, eV_s typically exceeds the bulk kinetic energy (E_k) of the ions, which on the other hand is larger than the thermal energy of the ions. The following inequality then exists:

$$kT_i < E_k < eV_s \quad (1)$$

where k is the Bolzmann constant, T_i is the ion temperature, e is the elementary charge and V_s is the spacecraft potential relative to the ambient plasma.

[23] As a consequence of the above condition, a wake void of ions forms behind the spacecraft [see, e.g., *Eriksson et al.*, 2006]. The far more mobile electrons, however, will be able to fill the wake. Consequently, the EFW double probe instrument detects an artificial electric field along the wake direction. Combined with the magnetic and the convection electric field, it is then possible to obtain the parallel velocity of the ions [see *Engwall et al.*, 2009a, Equation (4)]. For approximately 180,000 records of the full EFW data set, it was possible to calculate the outflow velocity by using this method.

[24] Since the velocity determination rests on identification of this wake, the method can be more sensitive to protons than to heavier ions. This tendency is usually weak, and any error in determined parallel flow velocity becomes significant only in special circumstances (the species have different parallel flow velocities at the same time as the oxygen flow kinetic energy is close to or above the energy required to overcome the spacecraft potential).

[25] *Engwall et al.* [2009b] estimated that the errors due to the methodology is of the order $\pm 40\%$ or less for the velocity calculations and less than $\pm 20\%$ for the electron density calculations. Although the actual ion composition can vary greatly with disturbance level [e.g., *Comfort and Horwitz*, 1981; *Lennartsson*, 1994; *Vaisberg et al.*, 1996; *Barakat and Schunk*, 2006], the uncertainty in ion density is exactly the same as for electron density, as long as ions are singly charged. For a more detailed description about the methodology to obtain the density and velocity, and its limitations and error bounds, we refer to papers by *Engwall et al.* [2006, 2009b], *Pedersen et al.* [2008], and *Lybekk et al.* [2012].

[26] The calculation of outflow velocity rests on the simultaneous availability of EDI and EFW data. So far, only data from Cluster SC3 for the years 2001–2005 have been processed. Still, the number of records is large enough to allow us to extract subsets within certain geomagnetic activity levels, IMF directions etc. to check correlations and dependencies.

[27] Figure 2 shows the distribution of density and velocity of the cold plasma outflow. The average (arithmetic mean) density is 0.18 ± 0.22 cm^{-3}, and the average outflow velocity is 26 ± 17.2 km s^{-1} (the spread in these numbers are the standard deviations). The corresponding median values are 0.10 cm^{-3} and 24 km s^{-1}, respectively. The spread in the data is thus comparable or larger than errors due to the methodology. Only a small fraction of the events have negative velocities, i.e., motion into the ionosphere. The large majority of the events indicate ion outflow, i.e, downtail evacuation of ionospheric plasma.

[28] The field aligned acceleration, also important for our calculation, is apparent from Figure 2 (bottom); we estimate an initial acceleration of the order of 0.6–0.7 km s^{-1}/R$_E$. The observed increase in velocity can probably be attributed to centrifugal acceleration. Other forces, such as gravity and mirror force do not play any role at these altitudes. *Cladis* [1986], *Cladis et al.* [2000], and *Nilsson et al.* [2008, 2010] have suggested that centrifugal acceleration can sometimes be significant, and may explain a large fraction of the parallel velocities observed at high altitude above the polar cap.

[29] As we shall discuss further in section 4, the convection is highly dependent on the IMF direction, whereas neither field aligned velocity nor density react that much to IMF changes on the timescales we consider. Due to the orbit of Cluster, we are not well suited to address seasonal dependencies. Most Cluster measurements from the lobe and tail are obtained during northern hemisphere summer (June to October). Also, since none of the data sets are continuous in time, we cannot say anything about time evolution on any timescale.

3.2. Convection Toward the Plasma Sheet

[30] Convection toward the plasma sheet using EDI data was studied in detail by *Haaland et al.* [2008, 2009], and we use the same data set for the present study. This data set consists of approximately 450,000 one minute averages (approx 7600 hours) of convection from the EDI instruments during the years 2001–2008.

[31] EDI measures the drift of the gyro center of an artificially emitted electron beam. For a given electron energy and a known homogeneous (within a gyro radius) magnetic field, the so-called drift step is a function of the electric field. The method works extremely well in regions of space with stable magnetic field and low ambient electron density such as the polar cap and lobe regions. Since both the magnetic field and the electron gyro time can be determined with high accuracy, measurement errors with this technique are negligible. Uncertainties in statistical averages therefore come almost solely from the spread of the measurements.

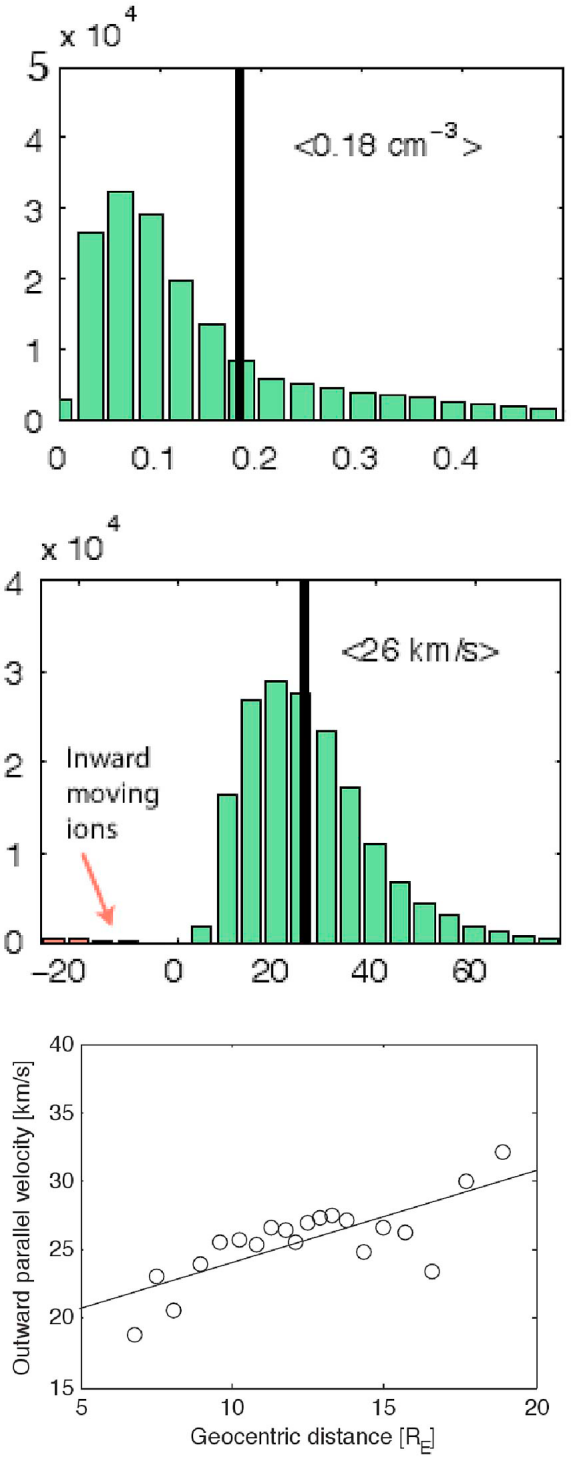

Figure 2. Data characteristics of the *Engwall et al.* [2009b] data set used in this paper. (top) Distribution of outflow densities. (middle) Distribution of outflow velocity, $V_{||}$. Horizontal axes show density and velocity, respectively, and vertical axes indicate number of samples. (bottom) Outflow velocity as function of altitude. The average outflow velocity increases approximately 10 km s^{-1} over a radial distance of 15 R_E.

[32] For a southward directed IMF, the variability in the convection data was found to be very low, with a well defined convection direction and magnitude. The flow is fairly homogeneous without any significant gradients or flow diversions, at least in the central lobes. For northward IMF conditions, the convection is more stagnant, and the spread in the data is comparable to the measurements itself. Since the convection velocities are vector quantities, there is spread in both magnitude and direction, and thus no single parameter describing the variability.

[33] For more details about the EDI instrument we refer to *Paschmann et al.* [2001]. A general discussion about variability and calculation of uncertainties in the EDI data set are given in *Haaland et al.* [2007] and *Förster et al.* [2007]. An assessment of the spread in magnitude and direction of the EDI data set used for this particular study is given in *Haaland et al.* [2008, Figure 4].

3.3. Polar Cap Area

[34] The size of the polar cap will greatly affect the total flux of outflowing ions. In *Engwall et al.* [2009b], the polar cap was defined as the area above 70° magnetic latitude. Possible expansions or contractions as a response to e.g., IMF changes or geomagnetic activity were not taken into account. Possible spatial inhomogeneities in the source area were also not considered in their study.

[35] We plan to address this issue in an upcoming paper (K. Li et al., On the ionospheric source region of cold ion outflow, submitted to *Geophysical Research Letters*, 2012), but for the present paper, we make use of the results from *Sotirelis et al.* [1998] to obtain a more realistic polar cap size. These results are based on characteristic particle signatures in the energy spectra from the low altitude DMSP satellites. In essence, the flux of energetic particles is much higher on closed field lines, and a sharp drop in intensity can be interpreted as a traversal from closed field lines (a trapped particle population) to open field lines (polar cap). The results from *Sotirelis et al.* [1998] demonstrate that both size and shape of the polar cap area can change dramatically, primarily as a response to the solar wind interaction with the dayside magnetopause. Figure 3, from *Sotirelis et al.* [1998], illustrates how the polar cap size varies as function of IMF Bz and the epsilon parameter, respectively.

[36] Figure 3 (top) shows the amount of open flux as function of IMF Bz and Figure 3 (bottom) shows open flux as function of the epsilon index. Using the same 1000 km altitude and an IGRF field magnitude of 37,000 nT as in *Engwall et al.* [2009b], we can derive the area of the polar cap as $A[m^2] = 2 * 1e9 * \Phi[Wb]/B[nT]$, where the factor 2 indicates that the area is calculated for both hemispheres. Since both the *Haaland et al.* [2008] and *Engwall et al.* [2009b] data sets contain both IMF and (indirectly) the epsilon parameter, we can consult Figure 3 to get an estimate of the polar cap area for any given value of IMF Bz or epsilon.

3.4. Example Calculation

[37] As an illustrative example, we use the average values from *Engwall et al.* [2009b] for outflow velocity, acceleration and density. We also use the average lobe convection measurements from *Haaland et al.* [2008]. Both data sets contain measurements from both the northern and southern

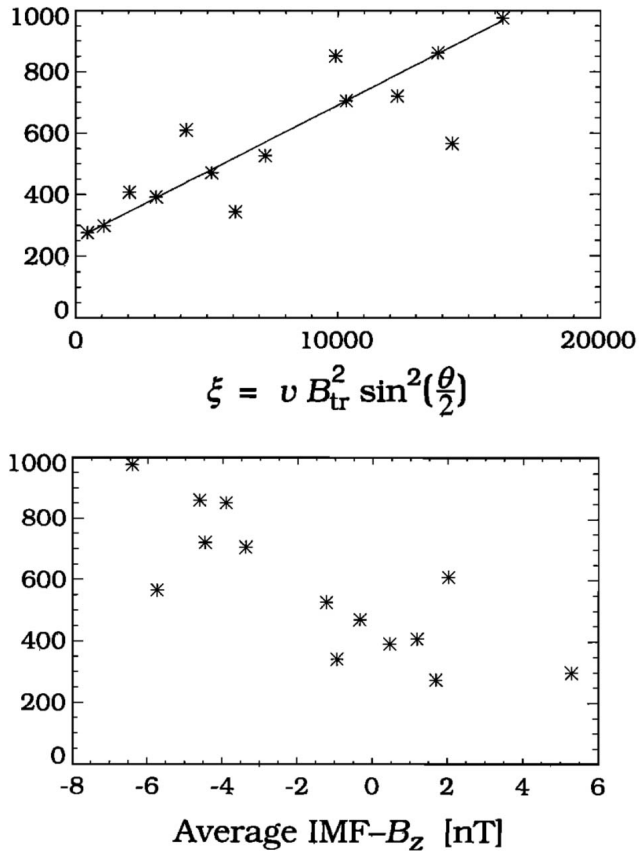

Figure 3. (top) Polar cap size (i.e., magnetic flux open field lines) in units of MWb as function of IMF Bz. (bottom) Same quantity, but now as function of a modified epsilon parameter. Enhanced dayside reconnection (larger negative Bz) and larger solar wind energy input lead to an expansion of the polar cap size. From *Sotirelis et al.* [1998].

hemisphere, but in this example calculation, we do not make any distinction between the two hemispheres. The combined (average of all values from both hemispheres) values are listed in Table 1.

[38] We also make use of calculations of acceleration and travel time presented in Figure 4. Figure 4 (top) shows the calculated velocity, $v(r) = v_0 + a(r)t$, of an ion as function of radial distance, r, up to 100 R_E (position of distant X-line). The measurements from *Engwall et al.* [2009b] (see Figure 2 (top)), taken at radial distances up to 20 R_E are overplotted as black dots. The extrapolation of these values out to the distant neutral line are calculated by assuming an initial acceleration $a = 0.7$ km s^{-1}/R_E, which reduces to essentially zero at larger distances ($a \propto r^{\gamma}$, where $\gamma = 0.9996$). An ion starting out with $v_0 = 25$ km s^{-1} at X = -10 R_E will then be accelerated and eventually reach velocities around 70 km s^{-1} near the distant X-line. This acceleration is consistent with the idea that the ions are exposed to centrifugal acceleration [*Cladis*, 1986; *Nilsson et al.*, 2008, 2010]. The acceleration will typically be strongest near the Earth where the magnetic field gradients are largest, but since centrifugal acceleration also depends on the convection speed, it may be overestimated in cases where the convection speed is small.

[39] Figure 4 (bottom) shows the travel time as function of tailward distance. The average ion will need approximately $T_x = 200$ min to travel from X = -10 R_E to X = -100 R_E. Assuming a constant convection with an average velocity of 7.5 km s^{-1}, the ion will be convected approximately 14 R_E toward the plasma sheet (i.e., essentially in $\pm Z_{GSE}$ direction) during these 200 min. Thus, ions flowing along field lines traversing X = -10 R_E more than 14 R_E above/below the plasma sheet will not be able to reach the plasma sheet before escaping beyond the distant neutral line. These ions will be directly lost into the solar wind.

[40] Depending on time of day, a field line traversing X = -10 R_E, Z_{GSE} = 14 R_E at local midnight, will have a foot point in the ionosphere somewhere between 76–86° corrected geomagnetic latitude (CGM) [see *Baker and Wing*, 1989]. Only ions escaping poleward of these latitudes, or from the dayside will be able to travel all the way downtail and escape into the solar wind.

4. Results

[41] The large data sets of *Engwall et al.* [2009b] and *Haaland et al.* [2009] allow for selection of subsets of the full data sets. In order to study e.g., the effect of geomagnetic activity or solar wind and IMF conditions, we extracted subsets of the outflow and convection data, containing only records within given ranges of the selected driver parameters.

[42] These subsets will typically have different average outflow velocities, acceleration, number densities and convection velocities. In addition, the polar cap area will change, and the location of the distant X-line may change.

4.1. Solar Wind and IMF Influence

[43] In order to assess the role of the IMF direction for the outflow and loss balance, we sorted the data sets into 4 bins according to IMF direction. Each bin contains data from a 90° clock angle sector centered around 0, 90, 180, 270° clock angle. Table 2 summarizes the average key parameters for each of these IMF bins. The average Dst, Pdyn and IMF values given are used to parameterize the magnetic field model used for mapping, and the velocities, densities and areas are used to calculate the outflow and direct loss. Keep in mind that we only discuss the direct loss into the solar wind along lobe field lines. Possible loss processes taking place after the ions have reached the plasma sheet, such as tailward retreat of a plasmoid, loss across the magnetopause, charge exchange or precipitation are not discussed.

[44] Table 2 reveals some interesting results. Whereas the convection varies from a few km s^{-1} for northward IMF to more than 12 km s^{-1} for southward IMF, neither outflow velocity nor density change dramatically with IMF direction.

Table 1. Data Set Characteristics With Averages of Some of the Key Parameters[a]

	Parameter	Value
$\langle V_{\parallel} \rangle$	average outflow velocity	25.7 ± 17.2 km s^{-1}
$\langle a_{\parallel} \rangle$	field aligned acceleration	0.6 km s^{-2}/R_E
$\langle N_e \rangle$	average outflow density	0.18 ± 0.22 cm^{-3}
$\langle V_{\perp} \rangle$	average convection velocity	7.0 km s^{-1}

[a]The spreads given are the standard deviation of the measurements. The acceleration is estimated from *Nilsson et al.* [2008], and the convection is taken from Table 2 in *Haaland et al.* [2008].

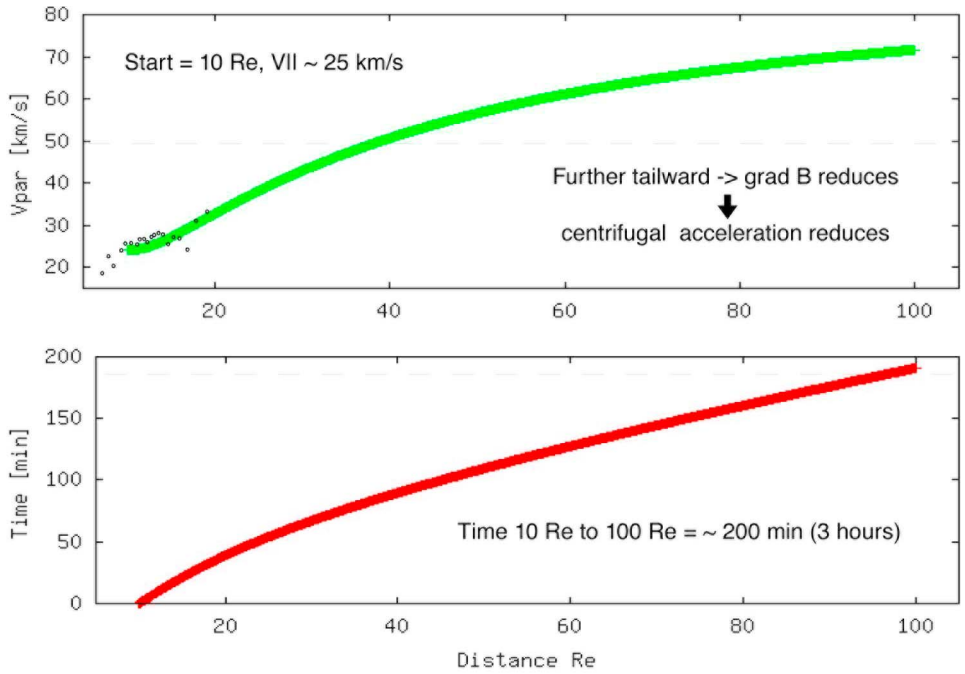

Figure 4. (top) Estimated field aligned velocity [km s^{-1}] as function of position. Ions starting out with the average field aligned velocity (25.7 km s^{-1}) and its rate of change with altitude given in *Engwall et al.* [2009b] will reach velocities of up to 70 km s^{-1} at 100 R_E distance. (bottom) Travel time (minutes) as function of position. The average travel time to the distant X-line at 100 R_E downtail, is estimated to be around 3 hours for this particular example.

[45] A northward directed IMF is associated with almost stagnant convection. During the approximately 3.5 hours it takes for an ion to travel along a field line from X = −10 R_E to the distant X-line 100 R_E downtail, the flux tube only convects around 3.4 R_E toward the plasma sheet. As a result, essentially all ions emanating from the polar cap are able to travel downtail and escape into the solar wind. Even X-line locations tailward of X = −200 R_E do not prevent ions from escaping downtail into the solar wind.

[46] A southward directed IMF, on the other hand, is associated with strong convection, mainly due to enhanced reconnection on the dayside magnetopause. During such conditions, essentially all ions are convected to the plasma sheet before reaching the distant neutral line and the direct loss is zero or negligible. By the same token, one can also argue that the supply of plasma of ionospheric origin is larger in the near Earth and mid-tail regions rather than in the distant tail; The fast convection will prevent ions from traveling far downtail before reaching the plasma sheet. Ions with high outflow velocity will be fed to the plasma sheet further downtail (see discussion in section 5.3). Since the outflow density, but also the total polar cap area is larger during southward IMF, the total outflow and thus supply to the plasma sheet are also much larger during southward IMF.

Table 2. Averages From the Data Set for Four Different Directions of the Interplanetary Magnetic Field

	Averages From *Engwall et al.* [2009b]							Calculated Values and Average Convection Velocity						
IMF[a]	Dst (nT)	Pdyn (nPa)	By (nT)	Bz (nT)	Ne (cm^{-2})	$V_{\|\|}$ (km s^{-1})	Flux (s^{-1} cm^{-2})	PCarea[b] (km^2)	OutFlow[c] (s^{-1})	T_X[d] (min)	$V_\perp$[e] (km s^{-1})	CD[f] (R_e)	LossArea[g] (km^2)	Lost[h] (s^{-1})
By+	−29.8	1.92	4.6	0.0	0.172	25.8	1.22e8	2.4e7	2.6e25	208	8.0	15.7	1.99e6	2.55e24
By−	−19.8	2.05	−5.4	−0.9	0.141	25.2	0.99e8	2.4e7	2.1e25	210	7.9	15.6	1.83e6	1.81e24
Bz−	−39.2	2.41	−0.4	−4.6	0.233	26.9	1.48e8	4.3e7	6.4e25	204	12.2	23.1	(0)[i]	(0)[i]
Bz+	−21.9	2.43	0.7	3.7	0.196	24.6	1.35e8	0.8e7	1.1e25	212	1.7	3.4	7.29e6	7.18e24

[a]90° sectors around 0, 90, 180 and 270° clock angles.
[b]Polar cap area - based on *Sotirelis et al.* [1998, Figure 9] and an IGRF field of 37,000 nT at 1000 km altitude.
[c]Total outflow = polar cap area multiplied by flux.
[d]Travel time along field from X_{GSE} = −10 Re to distant X-line assumed to be located at 100 R_E.
[e]Average convection velocity toward the plasma sheet based on the *Haaland et al.* [2008] data set.
[f]Convection distance - distance a field line convects during the travel time in [4] (see Figure 4).
[g]Loss area - part of polar cap where outflowing ions are lost downtail - see Figure 1.
[h]Direct loss into the solar wind only. Other losses, e.g., plasmoid escape, charge exchange, etc. are not included.
[i]See text.

Table 3. Averages From the Data Set for Three Different Geomagnetic Activity Levels

Averages From *Engwall et al.* [2009b]								Calculated Values and Average Convection Velocity						
Activity[a]	Dst (nT)	Pdyn (nPa)	By (nT)	Bz (nT)	Ne (cm^{-2})	$V_{\|\|}$ (km s^{-1})	Flux (cm^{-2})	PCarea[b] (km^2)	OutFlow[c] (s^{-1})	T_X[d] (min)	$V_\perp$[e] (km s^{-1})	CD[f] (R_e)	LossArea[g] (km^2)	Lost[h] (s^{-1})
Storm	−43.0	2.24	1.4	−1.4	0.209	28.1	1.48e8	2.84e7	4.20e25	200	10.1	19.0	1.13e6	1.68e24
Moderate	−10.4	1.77	−0.5	−0.5	0.127	23.3	0.87e8	2.43e7	2.11e25	217	6.9	14.1	8.85e6	7.44e24
Quiet	7.5	3.02	−1.2	0.5	0.184	23.1	1.21e8	2.16e7	2.61e25	218	4.5	9.2	2.07e7	2.51e25

[a]Quiet = Dst ≥ 0, Moderate = Dst between −20 and 0, Storm = Dst below −20 nT.
[b]Polar cap area - based on Figure 3 with an IGRF field of 37,000 nT at 1000 km altitude.
[c]Total outflow = polar cap area multiplied by flux.
[d]Travel time along field from $X_{GSE} = -10$ Re to distant X-line.
[e]Average convection velocity toward the plasma sheet based on the *Haaland et al.* [2008] data set.
[f]Convection distance - distance a field line convects during the travel time in [4] (see Figure 4).
[g]Loss area - part of polar cap where outflowing ions are lost downtail - see Figure 1.
[h]Direct loss into the solar wind only. Other losses, e.g., plasmoid escape, charge exchange, etc. are not included.

[47] We should here once again emphasize that all losses given in Table 2 only incorporate the direct loss along field lines with one foot point in the solar wind. In particular during southward IMF, a secondary X-line may form closer to Earth (typically 20–30 R_E downtail - see section 5.2), where parts of the plasma sheet are pinched off and ejected tailward. This process will also constitute a loss of cold plasma downtail. To avoid giving the impression that there is no loss of plasma into the solar wind for southward IMF, we have put the zero values in Table 2 in parentheses and attached a footnote to them.

[48] A By dominated IMF still has a fairly strong convection toward the plasma sheet, and the tailward loss is minimal. The polar cap area is about half of that for southward IMF, and the outflow density and outflow velocities are lower than for a purely southward IMF. The total outflow is therefore smaller than for southward IMF. From the data, we find a slightly higher flux for positive IMF By than for negative By values whereas the polar cap areas for the two IMF orientations are comparable.

[49] It should be pointed out that the above sorting is done according to the concurrent upstream IMF orientation. Since the data are not continuous in time, the effect of the IMF history cannot be investigated. It is plausible that e.g., an extended period of northward IMF will lead to a larger contraction of the polar cap [see, e.g., *Zhang et al.*, 2009], and lower outflow and densities than indicated in Table 2.

4.2. Response to Geomagnetic Activity Level

[50] The *Engwall et al.* [2009b] data includes the auroral electrojet (AE), the Disturbed Storm Time (Dst) and the K Planetary (Kp) indices used to describe the geomagnetic activity of the magnetosphere. Similarly, the *Haaland et al.* [2008] data set contains the AE and Dst indices. As a rule of thumb, AE describes auroral activity with timescales of minutes or hours. The mechanisms responsible for AE perturbations are field aligned currents arising from bursty bulk flow events and substorm activity in the central plasma sheet. The Dst index describes the global storm activity with timescales of hours to days, and is primarily a measure of the enhanced ring current. Due to the long transport times involved in cold ion outflow and a focus on the polar cap rather than the auroral zone, the Dst index is more suitable as an indicator of geomagnetic activity for our purpose.

[51] Table 3 is similar to Table 2, but now shows the corresponding outflow density, outflow velocity, convection velocity as well as the calculated quantities for three different disturbance conditions.

[52] For storm time periods (here defined as Dst ≤ −20 nT to get reasonable statistics), the outflow density and velocity are higher whereas the polar cap is more expanded compared to quiet and moderate conditions. The flux and total outflow are therefore correspondingly higher. At the same time, disturbed magnetospheric conditions are associated with enhanced convection. Thus, the total direct tailward loss is still minimal - the majority of the outflowing ions are recirculated during storm time conditions. Since near Earth reconnection is more likely to occur during storm time conditions, loss of cold plasma through escaping plasmoids may still occur though.

[53] Moderate conditions (Dst in the range between −20 and 0 nT), are characterized by a lower density and therefore a lower flux than storm periods. The polar cap area is also less expanded. Still, since the convection toward the plasma sheet is much lower than during storms, the direct net tailward loss is still larger.

[54] For quiet conditions (Dst values above 0 nT), the outflow density seems to be higher than during moderate disturbance levels. A higher polar cap density during positive Dst values was also noted by *Svenes et al.* [2008] and *Haaland et al.* [2012], and is probably related to a inward motion of the magnetopause and hence a compression of the magnetosphere, rather than an additional supply of plasma. The convection is more stagnant, and the total loss is therefore larger than for moderate and disturbed conditions.

4.3. Effects of Solar Activity

[55] Earlier studies [e.g., *Laakso et al.*, 2002; *Kitamura et al.*, 2011, and references therein] have demonstrated that solar illumination is the most significant driver of ionization in the ionosphere. Studies by *Svenes et al.* [2008] and *Lybekk et al.* [2012] show that enhanced ionization also leads to enhanced density of cold plasma in the polar cap and lobe regions. Interestingly, recent results by *Glocer et al.* [2012] also indicate that photoelectrons produced by solar illumination can also have an effect on the composition of outflowing ions.

[56] In addition to the obvious dayside versus nightside asymmetries in illumination, there is also time variation in the ionization due to changes in solar irradiance. A frequently used indicator of solar activity is the F10.7 index - a daily proxy for the total emission from the solar disc in the 10.7 cm

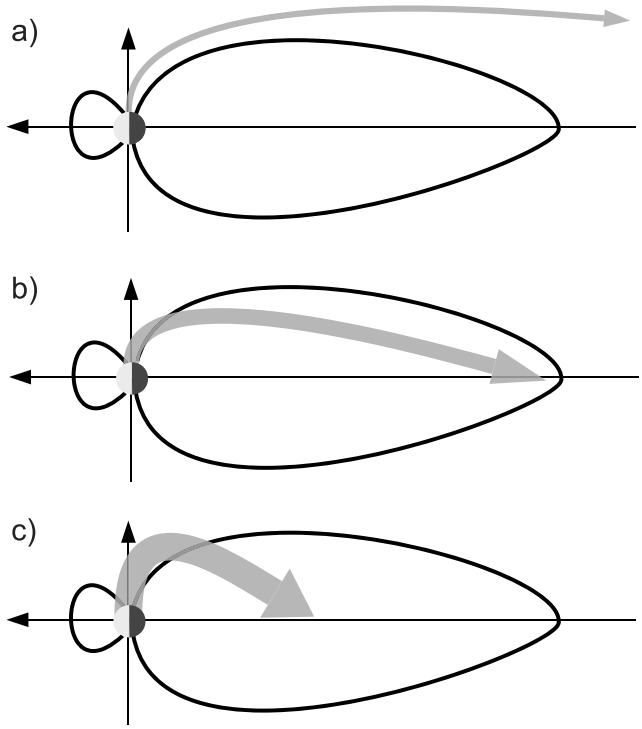

Figure 5. Typical trajectories of cold ions for different disturbance levels. Thickness of arrows indicate flux. (a) Stagnant convection, typically northward IMF conditions and low geomagnetic activity. The outflow flux and velocity is low, and outflowing ions will be lost directly downtail to the solar wind. (b) Low to intermediate convection: Outflowing ions will be transported far downtail before reaching the plasma sheet. (c) Strong convection, typically associated with strong dayside reconnection and disturbed magnetospheric conditions. Outflowing ions will be returned to the plasma sheet closer to Earth.

wavelength band. The *Engwall et al.* [2009a] data spans almost half a solar cycle and contains F10.7 values between 100 and 285. Their Figure 9 indicate an increase in the flux of cold ions by a factor of 3 between the lowest and highest F10.7 values. Since there is no discernible correlation between solar irradiance and convection, the corresponding recirculation and downtail loss also vary accordingly.

5. Discussion

5.1. Location of Distant X-Line

[57] A key parameter in our model is the position of the distant X-line. Ions able to travel beyond the distant X-line position before reaching the plasma sheet are directly lost to the solar wind in our scenario. The $X = -100\ R_E$ position is based on the results by *Daly* [1986], *Birn et al.* [1992] and more recent results by *Grigorenko et al.* [2009]. Other observations suggest that the X-line may retreat even further downtail under geomagnetically active periods [e.g., *Nishida et al.*, 1996, and references therein].

[58] As seen from Table 2 and also discussed in the next section, southward IMF conditions are typically associated with high convection velocities, and the outflowing ions are brought to the plasma sheet well inside the $X = -50\ R_E$. Conversely, during northward IMF, the convection is nearly stagnant, and even an X-line location tailward of $X = -200\ R_E$ does not prevent the outflowing ions from escaping downtail. The X-line location is thus primarily important for intermediate geomagnetic conditions.

[59] In general, an X-line location further tailward means that the ions will have to travel further downtail, and thus have to spend more time in the lobes where they are exposed to convection. The net effect is a larger recirculation and lower tailward escape. Using the average values from section 3.4, but now assuming an X-line location of 150 R_E downtail, we find that an ion will need almost 300 min travel time. During these 300 min, the 7.5 km s^{-1} convection velocity will transport the field line ca 21 R_E toward the plasma sheet, and only ions escaping the polar caps at very high latitudes (above ca 81°CGM latitude) or from the dayside will be able to travel beyond the X-line and escape into the solar wind.

5.2. Near Earth Reconnection

[60] In addition to the reconnection process forming the distant neutral line, reconnection and X-line formation also take place closer to Earth. Near Earth reconnection typically occurs during periods with southward IMF and is associated with bursty bulk flow and substorm activity. In this process, a fraction of the plasma sheet may be pinched off and ejected downtail as a plasmoid. However, the simple 2D picture of a near Earth neutral line and subsequent tailward retreating plasmoid (schematically illustrated in *Hones* [1979], for example), is probably quite far from reality. Recurrence rate, duration and scale sizes of near Earth reconnection are still debated (see, e.g., recent discussions in *Newell and Gjerloev* [2011], and references therein. Studies based on GEOTAIL [*Nagai et al.*, 1997] and more recent THEMIS observations [*Imber et al.*, 2011] indicate that reconnection typically initiates around 20–30 R_E downtail, although observations of reconnection around $X = -10\ R_E$ or less also exists [e.g., *Miyashita et al.*, 2005; *Du et al.*, 2011].

[61] One could argue that a tailward escaping plasmoid constitute a significant loss of cold plasma downtail into the solar wind. On the other hand, one should also keep in mind that ions convected to the plasma sheet may also eventually be lost through various processes (escape across the magnetopause, charge exchange, precipitation etc.). With the present data set, we are not well suited to address theses losses, thus the emphasis on *direct* loss in this paper.

5.3. Ion Outflow Feeding the Plasma Sheet

[62] From the results in section 4, we can conclude that the fate of the outflowing ions is mainly controlled by the convection, which again is primarily driven by the dayside reconnection. Whereas the convection can vary from essentially zero to several 10's km s^{-1}, the outflow parallel transport varies much less (see Figure 2). An interesting consequence of this is that the convection will also strongly influence *where* in the plasma sheet the recirculated cold ions will end up.

[63] Figure 5 illustrates the typical transport for different magnetospheric conditions. As illustrated in Figure 5a, and also apparent from Table 2, stagnant convection will lead to substantial direct loss downtail. This also holds if the X-line is located much further tailward than our assumptions.

[64] The Cluster measurements of cold plasma outflow suggest that the outflow never completely subsides [see *Engwall et al.*, 2009b, Figures 10 and 11]. As long as there is some convection toward the plasma sheet, this means that there is always some supply of cold plasma to the plasma sheet. Moderate convection velocities (a few km s^{-1}), will allow the ions to travel far downtail before reaching the plasma sheet (Figure 5b). When the ions eventually interact with the sharp reversal of the magnetic field in the tail midplane, they will be scattered and energized. Simulations have demonstrated that the closer this interaction takes place to the X-line, the larger energization [e.g., *Ashour-Abdalla et al.*, 1993, and references therein]. Ions fed at large downtail distances will spend more time in the plasma sheet where they are accelerated.

[65] During periods of strong convection, on the other hand, most of the outflowing cold plasma will be supplied closer to the Earth (illustrated in Figure 5c). With average outflow velocities around 25–30 km s^{-1} and convection velocities exceeding 15 km s^{-1}, essentially all ions are convected to the plasma sheet inside 50 R_E. These ions spend less time in the plasma sheet, and will thus be less energized than ions supplied further downtail. Ions with very low outflow velocities will even be convected directly to the plasmasphere without undergoing any significant energization in the tail at all.

[66] In this sense, our results are largely in agreement with the POLAR results reported by *Moore et al.* [1999], although their observations were based on particle measurements with energies up to 450 eV, with much higher average outflow velocities.

6. Summary and Conclusion

[67] We have combined the results from *Engwall et al.* [2009b] discussing density and outflow velocities of cold plasma and the results of *Haaland et al.* [2008, 2009], discussing convection in the lobes.

[68] Both data sets span a wide range of geomagnetic activity levels and solar wind conditions, which allows for sorting into subsets. From these data sets, we have quantified the direct loss and recirculation of the outflowing cold ions for different geomagnetic conditions. The results can be summarized as following:

[69] 1. On average, about 10% of the outflowing cold ions detected by Cluster at 6–20 R_E altitude (i.e., about 10^{25} ions/s) are directly lost into the solar wind. The remaining part is recirculated within the magnetosphere and thus participates in the formation of the hot plasma sheet and eventually ring current plasma populations.

[70] 2. The direct tailward loss of cold ionospheric plasma is largely governed by the convection and to some extent by the polar cap size (source area).

[71] 3. The density and outflow velocities do not respond very much to IMF changes on short timescales, whereas convection is largely controlled by IMF direction.

[72] 4. For northward IMF, almost all outflowing cold ions are lost into the solar wind due to the stagnant convection. However, due to the contracted polar cap, the total outflow is lower than during other IMF directions.

[73] 5. For southward IMF, there is strong convection, and essentially all outflowing ions are fed to the plasma sheet (where they may eventually be lost through other processes).

[74] 6. Geomagnetic active periods (storms) are associated with a larger outflow flux, but also a stronger convection and thus a higher circulation.

[75] 7. High solar activity is associated with larger EUV ionization and higher densities. Both loss and circulation increase accordingly.

[76] **Acknowledgments.** Computer code used for the calculations in this paper has been made available as part of the QSAS science analysis system. QSAS is provided by the United Kingdom Cluster Science Centre (Imperial College London and Queen Mary, University of London) supported by the United Kingdom Science and Technology Facilities Council (STFC). Solar wind data were obtained from the Coordinated Data Analysis Web (CDAWeb - see http://cdaweb.gsfc.nasa.gov/about.html). We thank the International Space Science Institute, Bern, Switzerland for providing computer resources and infrastructure for data exchange.

[77] Masaki Fujimoto thanks the reviewers for their assistance in evaluating this paper.

References

André, M., and C. M. Cully (2012), Low-energy ions: A previously hidden solar system particle population, *Geophys. Res. Lett.*, *39*, L03101, doi:10.1029/2011GL050242.

Ashour-Abdalla, M., J. P. Berchem, J. Büchner, and L. M. Zelenyi (1993), Shaping of the magnetotail from the mantle: Global and local structuring, *J. Geophys. Res.*, *98*, 5651.

Axford, W. I. (1968), The polar wind and the terrestrial helium budget, *J. Geophys. Res.*, *73*, 6855.

Baker, K. B., and S. Wing (1989), A new magnetic coordinate system for conjugate studies at high latitudes, *J. Geophys. Res.*, *94*, 9139.

Barakat, A. R., and R. W. Schunk (2006), A three-dimensional model of the generalized polar wind, *J. Geophys. Res.*, *111*, A12314, doi:10.1029/2006JA011662.

Birn, J., G. Yur, H. U. Rahman, and S. Minami (1992), On the termination of the closed field line region of the magnetotail, *J. Geophys. Res.*, *97*, 14,833.

Chappell, C. R., T. E. Moore, and J. H. Waite Jr. (1987), The ionosphere as a fully adequate source of plasma for the Earth's magnetosphere, *J. Geophys. Res.*, *92*, 5896.

Chappell, C. R., B. L. Giles, T. E. Moore, D. C. Delcourt, P. D. Craven, and M. O. Chandler (2000), The adequacy of the ionospheric source in supplying magnetospheric plasma, *J. Atmos. Sol.-Terr. Phys.*, *62*, 421.

Cladis, J. B. (1986), Parallel acceleration and transport of ions from polar ionosphere to plasma sheet, *Geophys. Res. Lett.*, *13*, 893.

Cladis, J. B., H. L. Collin, O. W. Lennartsson, T. E. Moore, W. K. Peterson, and C. T. Russel (2000), Observations of centrifugal acceleration during compression of magnetosphere, *Geophys. Res. Lett.*, *27*, 915.

Comfort, R. H., and J. L. Horwitz (1981), Low energy ion pitch angle distributions observed on the dayside at geosynchronous altitudes, *J. Geophys. Res.*, *86*, 1621.

Daly, P. W. (1986), Structure of the distant terrestrial magnetotail, *Adv. Space Res.*, *6*, 245.

Du, A. M., et al. (2011), Fast tailward flows in the plasma sheet boundary layer during a substorm on 9 March 2008: THEMIS observations, *J. Geophys. Res.*, *116*, A03216, doi:10.1029/2010JA015969.

Engwall, E., A. I. Eriksson, M. André, I. Dandouras, G. Paschmann, J. Quinn, and K. Torkar (2006), Low-energy (order 10 eV) ion flow in the magnetotail lobes inferred from spacecraft wake observations, *Geophys. Res. Lett.*, *33*, L06110, doi:10.1029/2005GL025179.

Engwall, E., A. I. Eriksson, C. M. Cully, M. André, P. A. Puhl-Quinn, H. Vaith, and R. Torbert (2009a), Survey of cold ionospheric outflows in the magnetotail, *Ann. Geophys.*, *27*, 3185.

Engwall, E., A. I. Eriksson, C. M. Cully, M. André, R. Torbert, and H. Vaith (2009b), Earth's ionospheric outflow dominated by hidden cold plasma, *Nat. Geosci.*, *2*, 24.

Eriksson, A. I., et al. (2006), Electric field measurements on Cluster: comparing the double-probe and electron drift techniques, *Ann. Geophys.*, *24*, 275.

Escoubet, C. P., A. Pedersen, R. Schmidt, and P. A. Lindqvist (1997a), Density in the magnetosphere inferred from ISEE 1 spacecraft potential, *J. Geophys. Res.*, *102*, 17,595.

Escoubet, C. P., R. Schmidt, and M. L. Goldstein (1997b), Cluster: Science and mission overview, *Space Sci. Rev.*, *79*, 11.

Förster, M., G. Paschmann, S. E. Haaland, J. M. Quinn, R. B. Torbert, H. Vaith, and C. A. Kletzing (2007), High-latitude plasma convection form cluster EDI: Variances and solar wind correlation, *Ann. Geophys.*, *25*, 1691.

Glocer, A., N. Kitamura, G. Toth, and T. Gombosi (2012), Modeling solar zenith angle effects on the polar wind, *J. Geophys. Res.*, *117*, A04318, doi:10.1029/2011JA017136.

Grigorenko, E. E., M. Hoshino, M. Hirai, T. Mukai, and L. M. Zelenyi (2009), Geography of ion acceleration in the magnetotail: X-line versus current sheet effects, *J. Geophys. Res.*, *114*, A03203, doi:10.1029/2008JA013811.

Gustafsson, G., et al. (2001), First results of electric field and density measurements by Cluster EFW based on initial months of operation, *Ann. Geophys.*, *19* , 1219.

Haaland, S., M. Förster, and G. Paschmann (2007), High-latitude plasma convection from cluster EDI measurements: Method and IMF-dependence, *Ann. Geophys.*, *25*, 239.

Haaland, S., G. Paschmann, M. Förster, J. Quinn, R. Torbert, H. Vaith, P. Puhl-Quinn, and C. Kletzing (2008), Plasma convection in the magnetotail lobes: statistical results from Cluster EDI measurements, *Ann. Geophys.*, *26*, 2371.

Haaland, S., B. Lybekk, K. Svenes, A. Pedersen, M. Förster, H. Vaith, and R. Torbert (2009), Plasma transport in the magnetotail lobes, *Ann. Geophys.*, *27*, 3577.

Haaland, S., K. Svenes, B. Lybekk, and A. Pedersen (2012), A survey of the polar cap density based on Cluster EFW probe measurements: Solar wind and solar irradiation dependence, *J. Geophys. Res.*, *117*, A01216, doi:10.1029/2011JA017250.

Hones, E. W., Jr. (1979), Transient phenomena in the magnetotail and their relation to substorms, *Space Sci. Rev.*, *23*, 393.

Imber, S. M., J. A. Slavin, H. U. Auster, and V. Angelopoulos (2011), A THEMIS survey of flux ropes and traveling compression regions: Location of the near-Earth reconnection site during solar minimum, *J. Geophys. Res.*, *116*, A02201, doi:10.1029/2010JA016026.

Kitamura, N., Y. Ogawa, Y. Nishimura, N. Terada, T. Ono, A. Shinbori, A. Kumamoto, V. Truhlik, and J. Smilauer (2011), Solar zenith angle dependence of plasma density and temperature in the polar cap ionosphere and low-altitude magnetosphere during geomagnetically quiet periods at solar maximum, *J. Geophys. Res.*, *116*, A08227, doi:10.1029/2011JA016631.

Laakso, H., R. Pfaff, and P. Janhunen (2002), Polar observations of electron density distribution in the Earth's magnetosphere. 1. Statistical results, *Ann. Geophys.*, *20*, 1711.

Lennartsson, O. W. (1994), Tail lobe ion composition at energies of 0.1 to 16 keV/e: Evidence for mass-dependent density gradients, *J. Geophys. Res.*, *99*, 2387.

Lockwood, M., J. H. Waite, Jr., T. E. Moore, C. R. Chappell, and M. O. Chandler (1985a), The cleft ion fountain, *J. Geophys. Res.*, *90*, 9736.

Lockwood, M., J. H. Waite, Jr., T. E. Moore, C. R. Chappell, and J. F. E. Johnson (1985b), A new source of suprathermal O(+) ions near the dayside polar cap boundary, *J. Geophys. Res.*, *90*, 4099.

Lybekk, B., A. Pedersen, S. Haaland, K. Svenes, A. N. Fazakerley, A. Masson, M. G. G. T. Taylor, and J.-G. Trotignon (2012), Solar cycle variations of the Cluster spacecraft potential and its use for electron density estimations, *J. Geophys. Res.*, *117*, A01217, doi:10.1029/2011JA016969.

Miyashita, Y., et al. (2005), Geotail observations of signatures in the near-Earth magnetotail for the extremely intense substorms of the 30 October 2003 storm, *J. Geophys. Res.*, *110*, A09S25, doi:10.1029/2005JA011070.

Moore, T., et al. (1999), Polar/TIDE results on polar outflows, in *Sun-Earth Plasma Connections*, *Geophys. Monogr. Ser.*, vol. 109, edited by J. L. Burch, R. L. Carovillano, and S. K. Antiochos, p. 87, AGU, Washington, D. C.

Moore, T. E., and J. L. Horwitz (2007), Stellar ablation of planetary atmospheres, *Rev. Geophys.*, *45*, RG3002, doi:10.1029/2005RG000194.

Moore, T. E., et al. (1995), The Thermal Ion Dynamics Experiment and Plasma Source Instrument, *Space Sci. Rev.*, *71*, 409.

Moore, T. E., et al. (1997), High-altitude observations of the polar wind., *Science*, *277*, 349.

Nagai, T., R. Nakamura, T. Mukai, T. Yamamoto, A. Nishida, and S. Kokubun (1997), Substorms, tail flows and plasmoids, *Adv. Space Res.*, *20*, 961.

Newell, P. T., and J. W. Gjerloev (2011), Substorm and magnetosphere characteristic scales inferred from the SuperMAG auroral electrojet indices, *J. Geophys. Res.*, *116*, A12232, doi:10.1029/2011JA016936.

Nilsson, H., et al. (2008), An assessment of the role of the centrifugal acceleration mechanism in high altitude polar cap oxygen ion outflow, *Ann. Geophys.*, *26*, 145.

Nilsson, H., E. Engwall, A. Eriksson, P. A. Puhl-Quinn, and S. Arvelius (2010), Centrifugal acceleration in the magnetotail lobes, *Ann. Geophys.*, *28*, 569.

Nishida, A., T. Mukai, T. Yamamoto, Y. Saito, and M. Kokubun (1996), Magnetotail convection in geomagnetically active times, 1. distance to the neutral lines, *J. Geophys. Geomagn.*, *48*, 489.

Paschmann, G., et al. (2001), The electron drift instrument on Cluster: Overview of first results, *Ann. Geophys.*, *19*, 1273.

Pedersen, A., F. Mozer, and G. Gustafsson (1998), Electric field measurements in a tenuous plasma with spherical double probes, in *Measurement Techniques in Space Plasmas – Fields*, *Geophys. Monogr. Ser.*, vol. 103, edited by R. F. Pfaff, J. E. Borovsky, and D. T. Young, p. 1, AGU, Washington, D. C.

Pedersen, A., P. Décréau, C. Escoubet, G. Gustafsson, H. Laakso, P. Lindqvist, B. Lybekk, A. Masson, F. Mozer, and A. Vaivads (2001), Four-point high time resolution information on electron densities by the electric field experiments (EFW) on Cluster, *Ann. Geophys.*, *19*, 1483.

Pedersen, A., et al. (2008), Electron density estimations derived from spacecraft potential measurements on cluster in tenuous plasma regions, *J. Geophys. Res.*, *113*, A07S33, doi:10.1029/2007JA012636.

Quinn, J. M., et al. (2001), Cluster EDI convection measurements across the high-latitude plasma sheet boundary at midnight, *Ann. Geophys.*, *19*, 1669.

Sotirelis, T., P. T. Newell, and C. Meng (1998), Shape of the open-closed boundary of the polar cap as determined from observations of precipitating particles by up to four DMSP satellites, *J. Geophys. Res.*, *103*, 399.

Su, Y.-J., J. L. Horwitz, T. E. Moore, B. L. Giles, M. O. Chandler, P. D. Craven, M. Hirahara, and C. J. Pollock (1998), Polar wind survey with the Thermal Ion Dynamics Experiment/Plasma Source Instrument suite aboard POLAR, *J. Geophys. Res.*, *103*, 29,305.

Svenes, K., B. Lybekk, A. Pedersen, and S. Haaland (2008), Cluster observations of magnetospheric lobe plasma densities for different solar wind conditions: A statistical study, *Ann. Geophys.*, *26*, 2845.

Tsyganenko, N. A. (2002a), A model of the near magnetosphere with a dawn-dusk asymmetry: 1. Mathematical structure, *J. Geophys. Res.*, *107*(A8), 1179, doi:10.1029/2001JA000219.

Tsyganenko, N. A. (2002b), A model of the near magnetosphere with a dawn-dusk asymmetry: 2. Parameterization and fitting to observations, *J. Geophys. Res.*, *107*(A8), 1176, doi:10.1029/2001JA000220.

Vaisberg, O. L., L. A. Avanov, J. L. Burch, and J. H. Waite (1996), Measurements of plasma in the magnetospheric tail lobes, *Adv. Space Res.*, *18*, 63.

Yau, A. W., and M. Andre (1997), Sources of ion outflow in the high latitude ionosphere, *Space Sci. Rev.*, *80*, 1.

Yau, A. W., L. Lenchyshyn, E. G. Shelley, and W. K. Peterson (1985), Energetic auroral and polar ion outflow at DE 1 altitudes: Magnitude, composition, magnetic activity dependence, and long-term variations, *J. Geophys. Res.*, *90*, 8417.

Zhang, Y., L. J. Paxton, P. T. Newell, and C.-I. Meng (2009), Does the polar cap disappear under an extended strong northward IMF?, *J. Atmos. Sol. Terr. Phys.*, *71*, 2006.